

Thermal infrared stellar interferometry using single-mode guided optics: first results with the TISIS experiment on IOTA

B. Mennesson¹, J.M. Mariotti^{1,2}, V. Coudé du Foresto¹, G. Perrin¹, S. Ridgway³, C. Ruilier¹, W.A. Traub⁴, N.P. Carleton⁴, M.G. Lacasse⁴, and G. Mazé⁵

¹ DESPA, Observatoire de Paris, F-92195 Meudon, France

² ESO, D-85748 Garching, Germany

³ National Optical Astronomy Observatories, Tucson, AZ 85726-6732, USA

⁴ Harvard-Smithsonian Center for Astrophysics, Cambridge, MA 02138, USA

⁵ Le Verre Fluoré, Campus Ker Lann, F-35170 Bruz, France

Received 14 October 1998 / Accepted 8 February 1999

Abstract. We report the first long baseline interferometric observations obtained in the thermal infrared with a single-mode fiber coupler. Stellar fringes have been found on α Bootis (Arcturus) and α Herculis, with a 21 m baseline of the Infrared and Optical Telescope Array (IOTA), located at the Smithsonian's Fred Lawrence Whipple Observatory (Mt Hopkins, Arizona). Beams from the telescopes are coherently combined through an X shaped fluoride glass single-mode fiber coupler. Although this device was not originally optimized for operation in the L band (effective wavelength of $3.75 \mu\text{m}$), we find good interferometric properties in that wavelength domain, with a rather high and steady instrumental transfer function, and very low dispersive effects. Observations are still limited by the poor sensitivity of the detectors and not by the thermal background, which was minimized. Visibilities derived from the interferograms are consistent with the published limb darkened diameters of α Herculis. It is, to our knowledge, the first time interferometric observations of Arcturus and α Her are reported in the L band.

Key words: instrumentation: interferometers – stars: fundamental parameters – stars: individual: α Her – stars: individual: Arcturus – infrared: stars

1. Introduction

Direct interferometry in the thermal infrared is planned for both ground based observations, with the 10 micron interferometric mode of the VLT (through its mid-infrared focal instrument, called “MIDI”, (Leinert & Graser 1998)), the 10 micron nulling mode on the Keck telescopes (Colavita 1998), and for space based projects mostly dedicated to the characterization of extrasolar planets, such as DARWIN (Léger et al. 1996) or TPF (Angel & Woolf 1997). High angular resolution in the mid-infrared is indeed required in various fields of astrophysics, from the observation and modeling of circumstellar dust shells around

late type stars, the study of young stellar objects (Natta 1997), of broad line regions of active galactic nuclei (Voit 1997), to the detection of key spectroscopic features in the atmosphere of extrasolar planets. Yet direct interferometry at wavelengths longer than 2.4 microns has been seldom demonstrated so far, and the problem of fringe visibility calibration in the thermal regime has never been addressed.

In the thermal infrared, ground based interferometric stellar observations face indeed very specific technical difficulties, when compared to the ones encountered in the visible or at near infrared ($\lambda < 2.4 \mu\text{m}$) wavelengths. The seeing is much better, and the constraints on the optical surfaces are relaxed, but the interferometric signal is contaminated by an incoherent thermal background, that needs to be minimized, monitored, and properly subtracted in order to achieve high accuracy visibility measurements. Around 10 microns, as discussed in Sect. 3.1, the thermal background signal is several orders of magnitude higher than the stellar flux itself. The difficulties in the alignment of the optics and the lower efficiency of the detectors are also probably responsible for the lack of interferometric observations in the thermal regime. First interferometric stellar observations were obtained by single aperture interferometry (McCarthy & Low 1975; McCarthy et al. 1977). First direct observations with separated apertures followed a decade later with the pioneer experiment of spatio-spectral interferometry conducted by Gay and Mekarnia at CERGA (Gay & Mékarnia 1988; Mékarnia & Gay 1990). But most of the scientific results derived from interferometric observations in the thermal infrared have been obtained through heterodyne interferometry at $11.15 \mu\text{m}$ (Danchi et al. 1994), studying dust shell properties of bright late type stars. Since only the coherent part of the light is coupled to a local oscillator, this latter technique provides visibility measurements which are relatively insensitive to seeing conditions and then more accurate. Although it has a better adaptability to multi-telescope combination, this technique has a low sensitivity for a small number of telescopes, limited by the narrow usable spectral bandwidth (about 6 GHz, i.e. a spectral resolution of about 5000 at 10 microns). Direct

Send offprint requests to: B. Mennesson

Correspondence to: bertrand@bluernote.obspm.fr

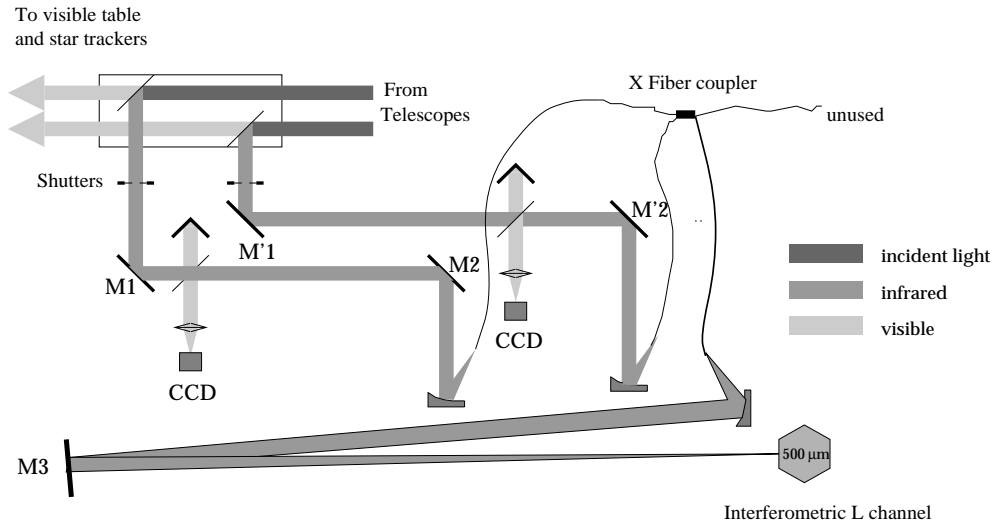


Fig. 1. Optical lay out of the TISIS combination table in the L band. A single X coupler is used for coherent combination of the beams coming from the 2 telescopes. There is only one interferometric output and no monitor of the signals coupled into the fibers.

broadband interferometry between large telescopes using adaptive optics and/or spatial filtering for real time correction of atmospheric effects, as planned for instance for the MIDI instrument, should lead to accurate visibility measurements and higher sensitivity. The expected background noise limited magnitude in the N band on two 8m telescopes is about 5, without integration capability, and could in principle reach 12 with a fringe tracker (Leinert & Graser 1998).

Interferometric observations in the L band reported here with the “TISIS” (Thermal Infrared Stellar Interferometric Setup) experiment face the specific problems of the thermal regime, under the less severe conditions of the 3.4–4.1 μm region. They constitute a first step towards future 10 micron observations and should help define signal processing procedures. More specifically, the aim of these observations is twofold:

1. To gain experience with the realm of long baseline direct interferometric observations in the thermal infrared, characterizing the intensity and time evolution of the thermal background.
2. To test single-mode components in this wavelength range, characterizing on the sky their transmission, dispersion and -to some extent- polarization properties. The use of spatial filters proves to be very helpful in order to derive accurate visibility measurements, (Perrin 1996; Coudé du Foresto et al. 1997) and would be of great use for the VLTI mid-infrared instrument (Leinert & Graser 1998). Spatial filtering is also very powerful to remove the high spatial frequency defects on the incoming wavefronts of a nulling interferometer (Ollivier & Mariotti 1997; Mennesson et al. 1998), which considerably relaxes the constraints on the optics.

Besides, observing in the L or M atmospheric windows has its own scientific interest by looking at structures around 1000 K, such as the inner edges of extended dust shells surrounding late type stars, as in the case of α Ceti or R Leo. Comparing these observations with photospheric measurements in K, and with former or simultaneous 10 μm heterodyne observations would

be of great interest in the modeling of complex shells around such objects. Coupling these thermal infrared data with quasi-simultaneous observations in the J,H and K bands obtained with the new IOTA NICMOS camera (Millan-Gabet 1998) would obviously also be very informative.

TISIS largely benefits from the FLUOR (Fiber Linked Unit for Optical Combination) optics (Coudé du Foresto et al. 1998), acquisition software, and reduction procedures (Coudé du Foresto et al. 1997) and uses the single mode fluoride glass couplers developed for FLUOR (Monerie et al. 1985), i.e. optimized for the K band. It also benefits from the whole infrastructure of the IOTA interferometer (Carleton et al. 1994). This enables us to concentrate on the issues specific to thermal infrared interferometry.

In the following sections we present the experimental context, from the IOTA environment to the fiber coupler. We give some instrumental results in relation with the two items above, and finally give visibility measurements on α Her, discussing related noise sources.

2. Experimental description

2.1. Experimental context

The observations were carried out with the two 45 cm telescopes of the IOTA interferometer located on Mount Hopkins, in Arizona. A complete updated description of IOTA is given by Traub (Traub 1998). The telescopes are made of a siderostat and a 1/10 afocal beam compressor. After compression, the direction of the beams is corrected for the rapid tip-tilt motion introduced by the atmosphere. This servo looped stabilization is based on the stellar image centroid position measured by visible star trackers, as presented in Fig. 1. One of the beams feeds a first (fixed) long delay line, that compensates for most of the external path difference, and then a second delay line with a shorter stroke and a very smooth motion to enable continuous modulation of the optical path difference during the observations. Thus the interferometer delivers in its central laboratory a pair of stabi-

lized and properly delayed afocal beams which in our case are combined on the TISIS table.

The telescopes can be relocated over an L shaped set of stations providing baselines ranging in length from 5 to 38 m. Observations were carried out with the South siderostat at its 15m station and the North siderostat at its 15 m station, so that the resulting baseline was 21 m long and quasi aligned with the North-South direction. As far as the interferometer is concerned, the only change with respect to observations in K is the removal of the windows (used to close the delay line and work under vacuum), due to their poor transmission above 3.5 microns. The delay line was then operated under atmospheric pressure.

2.2. Optical layout of the TISIS combination table

The optical scheme for combination in TISIS (Fig. 1) is a simplified version of the FLUOR instrument. Nevertheless a few differences can be noted in the optical arrangements of TISIS:

Fluctuations of the injection efficiency are not monitored at each input fiber, as should be done for optimum accuracy in the visibility computation. A few couplers available from the FLUOR K band experiment were tested and the only one properly balanced with respect to the two input signals in L is an X coupler with a broken output (a ‘‘Y’’ coupler). There is then only one usable -interferometric- output.

There is no polarization control through macrobending of the fibers. In the X-shaped coupler, originally designed and optimized for operation in the K band, the cutoff wavelength of the fundamental guided mode is $1.9 \mu\text{m}$. For a radiation with a wavelength typically twice as long, light is not guided as well (Neumann 1988), and important losses occur if the fiber is substantially bent. Consequently, the fibers are just kept as straight as possible to avoid additional losses.

Care has to be taken in order to limit the amount of thermal background received by the detector. A 2 mm cold field stop is then used in order to control the beam etendue, and the corresponding background seen by the detector. A Fabry lens located inside the cold part of the detector is used to reimage the fiber’s output on the diaphragm and insure a good filling of the detector’s InSb photodiode. With this optical arrangement, the beam etendue seen is defined as the product of the cold aperture area by the acceptance solid angle of the detector ($f/130$). This is equivalent to $10 \lambda^2$ at the center of the L band. In comparison, because of the single-mode character of the fibers, the starlight beam etendue seen by the detector is restricted to λ^2 , which corresponds to the diffraction limited case. The $10 \lambda^2$ beam etendue seen by the detector already keeps the background fluctuations below dark current noise (Sect. 3.1.1). Reducing it further to λ^2 would require a still smaller field stop, and very constraining optical alignments in order to keep the starlight on the detector.

We had to use an electrical offset before signal amplification in order to avoid saturation. The overall detection scheme is summarized in Fig. 2.

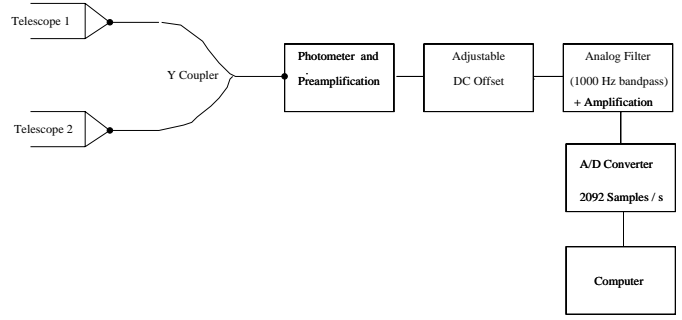


Fig. 2. Detection scheme

2.3. Observing procedure

Interferograms are obtained as scans around the zero optical path difference. For all the observations the speed of the delay line is set in order to yield an overall fringe speed of 1.5 mm/s, so that the apparent mean fringe frequency is about 400 Hz, and the analog filter cutoff frequency is set to 1000 Hz. Let us define the 4 independent sources of signal as i_{dc} , i_{th} , i_{sh} and i_{star} which stand respectively for the detector dark current, the overall thermal background (due to the sky and the warm optics), the shutter signal (thermal emission of the shutters and downstream warm optics) and the stellar signal. For each star, a few batches of 100 scans (~ 1 s long) are recorded. In a scan, half of the time is effectively used for stellar interferometric measurements, corresponding to a voltage $U_{star}(t)$ given by:

$$U_{star}(t) = g.(i_{dc} + i_{th} + i_{star}) \quad (1)$$

where g is the overall gain of the detection process. During the second part of a scan, shutters (see Fig. 1) are closed in the two interferometric arms, and we record the signal:

$$U_{sh}(t) = g.(i_{dc} + i_{sh}) \quad (2)$$

Ideal background measurements would require fast chopping or nodding on the sky. Since no chopping mode is available yet on IOTA, stellar observations are bracketed by sky observations, pointing towards a direction a few arcseconds away from the star. These sky measurements consist in two batches of 100 scans each, taken roughly 8 mn before and 8 mn after stellar acquisitions, and providing the signals $U_{sh}(t')$, and:

$$U_{sky}(t') = g.(i_{dc} + i_{th}) \quad (3)$$

Fig. 3 shows the various signals recorded: the stellar interferometric raw signal $U_{star}(t)$, and for comparison the scans obtained when shutter are closed ($U_{sh}(t)$) and while pointing the sky ($U_{sky}(t')$). In order to estimate the mean sky level at time of stellar observations t , the shutter signal is used as a common reference. The stellar contribution is estimated through the difference:

$$\begin{aligned} g(i_{star}(t)) &= U_{star}(t) - U_{sky}(t) \\ &\simeq (U_{star}(t) - U_{sh}(t)) + (U_{sh}(t') - U_{sky}(t')) \end{aligned} \quad (4)$$

The validity of this method obviously depends on the stability of the difference between sky and shutter signals recorded before

Table 1. Theoretical intensity of the thermal background in various standard photometric bands. The overall emissivity of warm optics is taken to be unity. Fluxes are computed for a 300 K source seen in one coherence etendue, i.e. a beam etendue of λ^2 , where λ is the mean wavelength of the spectral band. The ratio of thermal to detector noises assumes a detector Noise Equivalent Power of $10^{-14} W.Hz^{-1/2}$ as expected with our current photometer for frequencies of a few hundred Hz. Last two lines give theoretical point source limiting magnitudes using single mode fibers on IOTA in the L, M and N bands. Assumptions are: telescope diameter of 45 cm, overall emissivity of 1, beam etendue seen by the detector of $10\lambda^2$, overall transmission (optics and detector) per arm of 1%, interferometric efficiency of 50%, and fringe frequencies of 200 to 500 Hz.

Spectral band	K	L	M	N
Thermal background power injected in λ^2 (in W)	$5.5 \cdot 10^{-15}$	$4.7 \cdot 10^{-12}$	$1.9 \cdot 10^{-11}$	$4.5 \cdot 10^{-9}$
Star equivalent magnitude for a 45 cm aperture	10.1	1.1	-0.4	-11.0
Thermal Background Noise Equivalent Power ($W.Hz^{-1/2}$)	$7.6 \cdot 10^{-19}$	$5.0 \cdot 10^{-16}$	$1.8 \cdot 10^{-15}$	$2.8 \cdot 10^{-13}$
Ratio of thermal to detector noise	$7.6 \cdot 10^{-4}$	$5.0 \cdot 10^{-2}$	0.18	28
Limiting mag. (N.E.P.= $10^{-14}W.Hz^{-1/2}$)	-1	-2.5	-3.5	-6
Limiting mag. (N.E.P.= $10^{-15}W.Hz^{-1/2}$)	1.5	0	-2.0	-6

and after stellar acquisitions. The stability observed is presented in Sect. 3.1.2., showing clearly that observations are detector noise limited, and that we actually sample detector drifts rather than background or sky changes.

3. Instrumental results

Results are given for the nights of April 2 and April 3 1998, and are consistent with each other.

3.1. Background characterization

In this section we estimate the amount of thermal background received by the detector, and quantify its estimated uncertainty at the time of stellar observations.

3.1.1. Intensity

As described above, the interferometric beam is seen by the detector with a beam etendue of roughly $10\lambda^2$. Assuming an overall emissivity of the warm optics of 1 and a transmission of the cold optics of 1, we find a maximum thermal background Noise Equivalent Power (N.E.P.) of $1.6 \cdot 10^{-15} W.Hz^{-1/2}$. For comparison the N.E.P. of the detector (measured around 300 Hz) is $10^{-14} W.Hz^{-1/2}$, i.e. six times larger, so our observations in the L band are presently limited by the detectors. Table 1 compares the amount of thermal background expected in the K, L, M and N photometric bands. Note that the detector's N.E.P. only depends on the fringe apparent frequency. As long as this frequency is set around a few hundred Hz in each spectral band, the detector's N.E.P. is then considered here as a constant versus wavelength in a first approximation.

3.1.2. Resulting sensitivity

The theoretical limiting magnitudes for observations of a point source with the TISIS experiment on IOTA can be estimated in the various spectral bands as presented in Table 1. These values are derived from the FLUOR detection and reduction strategy (Coudé du Foresto 1997), taking a signal to noise ratio of 5 on each single measurement of the visibility squared modulus,

assuming a beam etendue seen by the detector of $10\lambda^2$, an overall transmission (optics and detector) per arm of 1%, and an interferometric efficiency of 50%. With the Noise Equivalent Power of our photometer ($\sim 10^{-14} W.Hz^{-1/2}$ for frequencies in the range of 200 to 500 Hz), we expect a theoretical limiting magnitude of -2.5 in the L band.

With a Noise Equivalent Power of $10^{-14} W.Hz^{-1/2}$ the detector noise dominates in L and M. With a detector of 10 times lower N.E.P. we should reach the thermal regime in the M band. In the N band, the thermal background is of course always dominant, and the sensitivity of the 45 cm siderostats is very low. The only candidates for observations in the N band have weak visible counterparts so that an infrared star tracker would be required.

A search for fringes on SW Vir, whose L magnitude is -2, was unsuccessful. α Her and Arcturus have respective magnitude -3.7 and -3.1 in L, so that the observed limiting magnitude is about -3 at the moment, which is in good agreement with theoretical expectations. Sensitivity can be improved using a fully transparent coupler in the L band, and detecting fringes on two complementary interferometric outputs. Less noisy detectors would also be very helpful, as Table 1 clearly shows.

3.1.3. Temporal fluctuations

- A slow parallel drift of the shutter and sky signals is observed, probably due to a slow drift of the detector inner temperature (Fig. 4a). The shutter signal effectively needs to be taken as a reference if one wants to estimate the background signal at the time of stellar observations.
- The difference between the sky and shutter signals is averaged over each scan (~ 1 s long), and ultimately over each consecutive batch of 100 scans. Fig. 4b shows the average level computed on such batches and the related error bars. In all cases the variation of the “sky-shutter” level between two consecutive batches bracketing stellar observations is small enough to estimate the average background level at the time of stellar interferometric observations within 1 mV. This error has to be compared with a stellar signal of typically 100 to 200 mV. We can then conclude that background

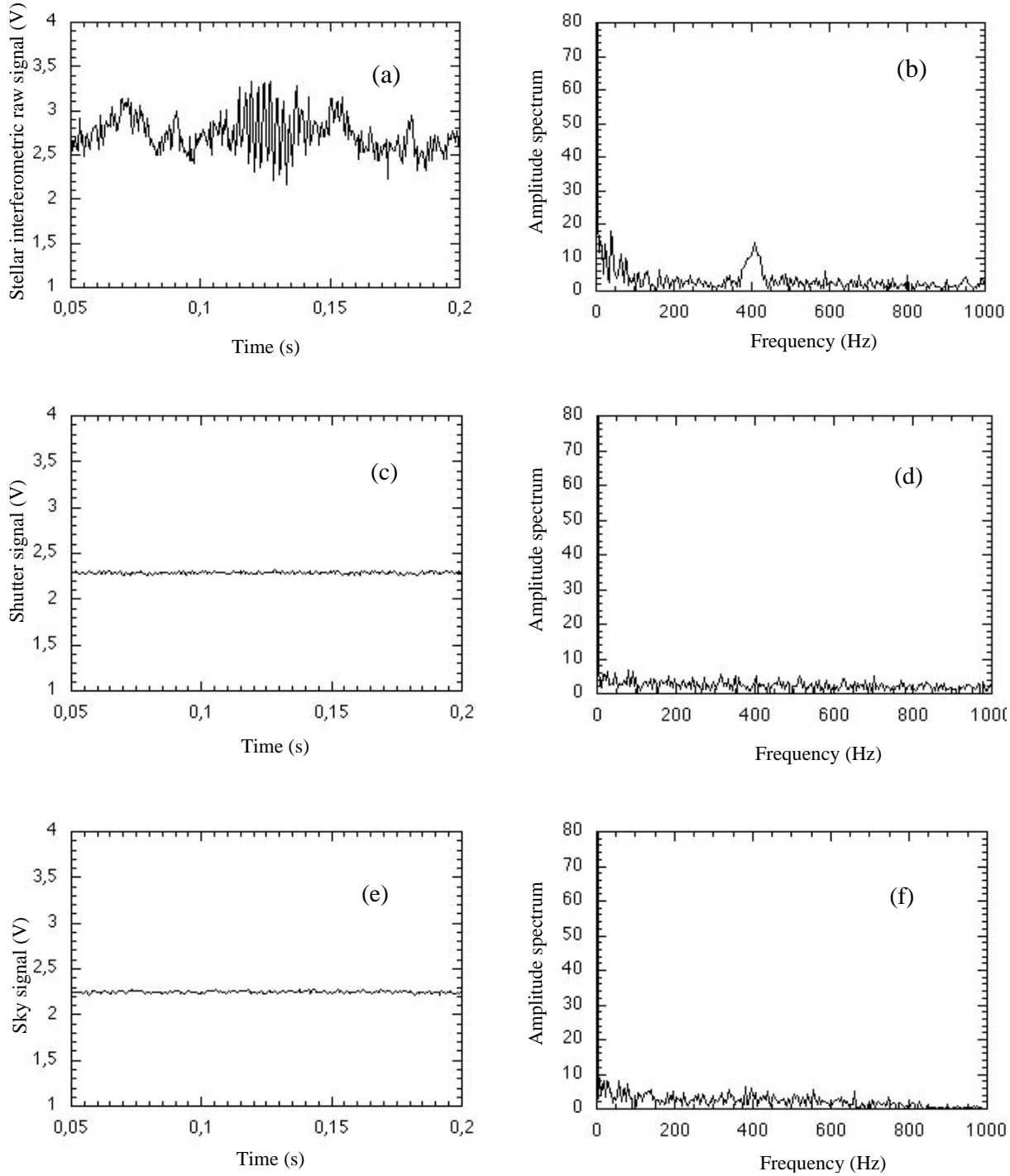


Fig. 3a–f. Typical recorded signals $U_{star}(t)$, $U_{sh}(t)$, $U_{sky}(t)$ (left panels **a**, **c** and **e**) and corresponding amplitude Fourier spectra (right panels **b**, **d** and **f** in arbitrary units). **a** Raw stellar interferogram obtained on αHer . Part of this signal located outside the fringe packet is used to characterize the coupling efficiency of the starlight into the single-mode coupler (Sect. 3.2). Plots **c** and **e** show for comparison the temporal scans obtained when shutters are closed, (“shutter signal $U_{sh}(t)$ ”), and when tracking a direction a few arcsecs away from the star (“sky signal $U_{sky}(t)$ ”).

fluctuations are correctly sampled and do not constitute a major source of uncertainty on visibility measurements, as discussed in Sect. 4.2.

- For each scan on the sky (250 ms long with an analog filter frequency of 1000 Hz) a Fourier transform is computed, and

its average value (on 600 independent scans) is plotted in Fig. 4d. It provides the high frequency part of the sky signal between 4 and 500Hz.

The low frequency part of the spectrum corresponds to the time evolution of the average of the scan signal, computed

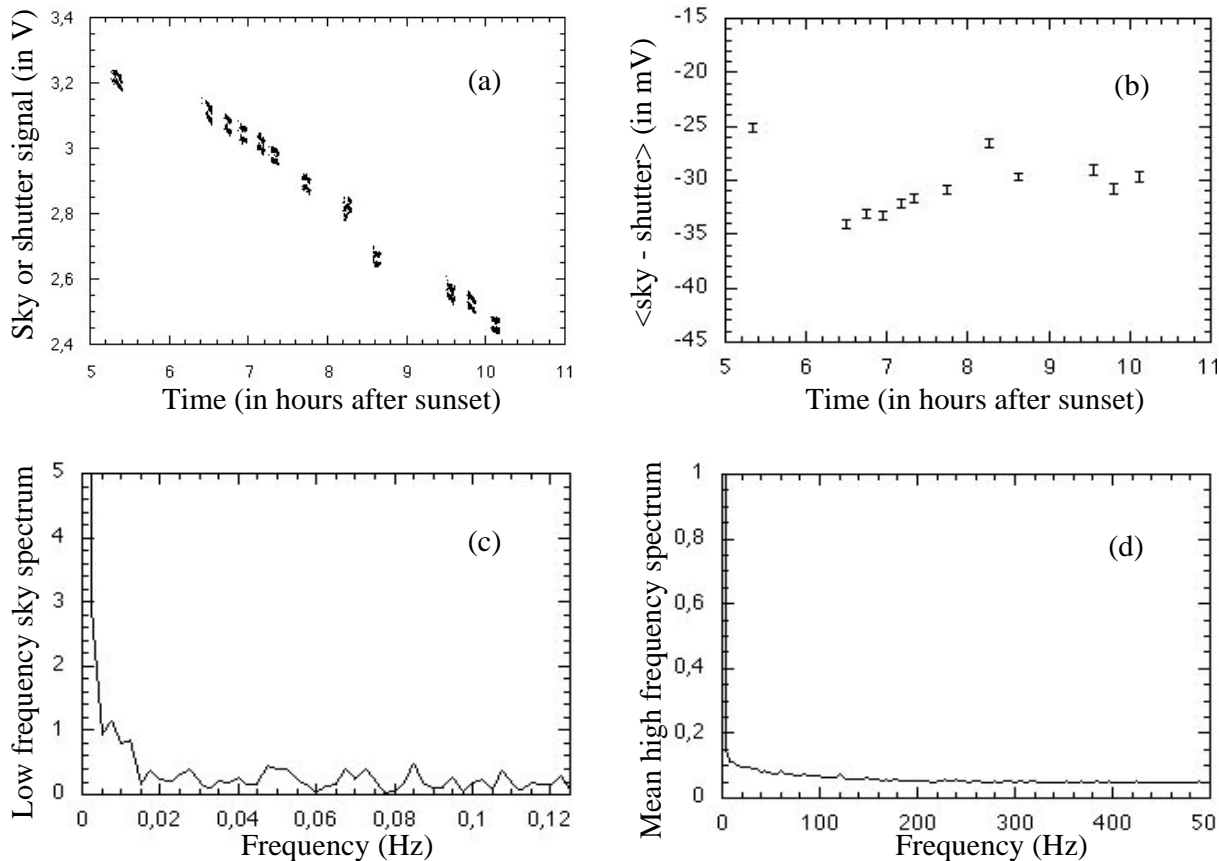


Fig. 4. **a** Temporal evolution of the shutter signal (upper points) and of the sky signal (lower points). Each point represents an average level over 250 ms. **b** Temporal evolution of the difference between the shutter and sky signals. Each point represents an average level over a batch of 100 scans. Error bars represent the standard deviation of the averaged scan level. **c** Amplitude spectrum of the low frequency part of the signal obtained from sky observations. **d** average amplitude spectrum of the high frequency part of the sky signal (same units as plot **a**). Note that the noise is reasonably flat for frequencies higher than 100 mHz, showing no peaks that might be confused with the fringe signal around 400 Hz.

every 4 seconds, on 100 scans. This gives access to the frequencies between 2.5 mHz and 125 mHz (Fig. 4c).

The analysis of these curves shows a rather sharp increase of the amplitude spectrum of the sky signal for frequencies lower than 15 mHz, which probably reflects the slow variations of the thermal background. The slowly decreasing and reasonably flat noise found for higher frequencies appears compatible with the hypothesis of a dominant detector noise. In any case chopping on the sky at reasonable rates (about 1 Hz) should remove most of the observed fluctuations.

3.2. Coupling efficiency

For a diffraction limited image formed at the focus of a telescope, the spatial distribution of the electric field scales proportionately with the wavelength, keeping the same profile (the Airy pattern, in a first approximation). Close enough to the cut-off wavelength (Neumann 1988) the fundamental mode of a single-mode fiber is described by a gaussian-like profile with its radius also roughly proportional to the wavelength. The theoretical coupling efficiency into the fiber is then achromatic in the absence of turbulence. With our fibers optimized for the K

band, the fundamental mode is not strictly gaussian in L, and the theoretical coupling efficiency is about 10% less in L than in K.

In presence of a turbulent atmosphere, the coupling efficiency is, to a first approximation, proportional to the Strehl ratio of the incoming wavefront. The former theoretical discrepancy of the coupling efficiency is then compensated by the improved seeing of the L band. More accurate calculations (Shaklan & Roddier 1988; Ruilier 1998) show that the injection efficiency should be roughly the same for the two wavelength domains, but that its time stability should be about 3 times better in the L band than in K.

On TISIS we can measure the stability of the injection into the fiber. A typical “interferometric” signal is given on Fig. 3a. Since there is no independent photometric measurement of the signals injected into each fiber, we use the incoherent addition of the two signals, as seen outside of the fringe packet, in order to probe the coupling efficiency of the starlight and its temporal evolution. The rms value of the fluctuations is 8% of the mean signal (the background has been subtracted). Assuming uncorrelated fluctuations of equal intensity at the two telescopes, we then estimate the relative variations of the coupling efficiency

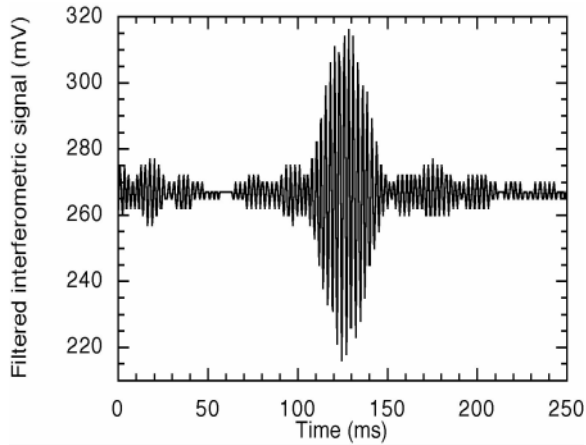


Fig. 5. Coherent addition of the signals injected by the two telescopes into the single mode coupler: a typical single-scan interferogram obtained on αHer , filtered at the optical bandpass. Resolution is limited on the temporal axis by the finite sampling rate (2092 Hz), and in the detected signals by the dynamic of the data acquisition board (2.4 mV of resolution).

at the focus of each telescope to be about 6%, which is indeed much better than what we usually get in the K band.

From these temporal fluctuations of the coupling efficiency, and depending on the number of turbulent modes corrected, we can theoretically (Shaklan & Roddier 1988; Ruilier 1998) estimate the turbulence strength, i.e. the Fried's parameter r_0 at the wavelength of observation. Assuming a perfect tip-tilt correction on a telescope of diameter D , we find $D/r_0 = 1.3$, and $D/r_0 = 0.3$ for uncorrected turbulence. Observations on IOTA are carried out in an intermediate regime with a partial tip-tilt correction, and then most probably at $D/r_0 < 1$ in the L band. This leads to a minimum value of 4 cm for the Fried's parameter at $0.5 \mu\text{m}$.

3.3. Characterization of the single mode coupler

3.3.1. Transmission

The transmission of the 2 m long single-mode X coupler is measured to be about 10% from one input to the single usable output, and 20% from the other input. Thus the split ratio of the coupler is 2 to 1, and it absorbs 85% of the energy over the whole spectral range of the L band. Since the chemical composition of the fiber and the geometry of the coupler were optimized for operation in the K band, this stronger attenuation in the L band was expected.

3.3.2. Dispersion

The ideal (zero dispersion) number of fringes expected with our L band filter ($\lambda_{mean} = 3.849 \mu\text{m}$, and $\Delta\lambda = 0.580 \mu\text{m}$) is about 13. Dispersion is quite low as indicated by the interferograms obtained on αHer (Fig. 5), numerically filtered at the fringe frequency, i.e. between 360 and 440 Hz, that shows roughly 16 fringes. Although the coupler used was optimized to

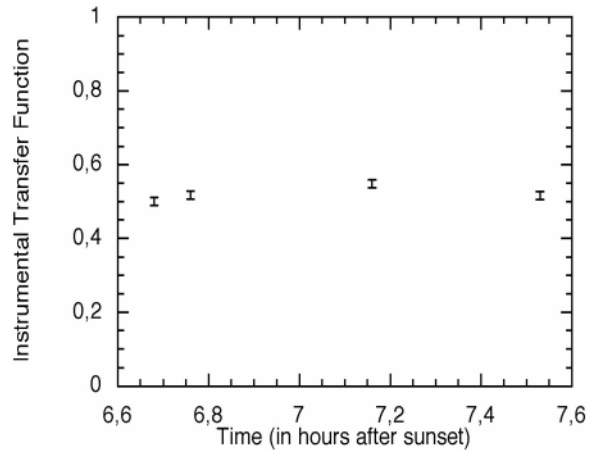


Fig. 6. Temporal evolution of the instrumental transfer function. First point is for the night of April 3, the other three points are for April 2 1998.

exhibit very low dispersive effects in the K band, this property appears to hold in L.

3.3.3. Interferometric efficiency

When single mode fibers are used for interferometric combination, visibility measurements can be corrected for atmospheric effects using either photometric derivations (so that further degradation of the interferometric efficiency is solely due to the instrumental transfer function, as in FLUOR), or the low frequency – photometric – part of the interferograms. This latter method is used for TISIS and leads to visibility measurements which are independent of atmospheric conditions to a good approximation (Coudé du Foresto et al. 1997). In what follows we then consider that interferometric efficiency and instrumental transfer function (T_i) are strictly equivalent and can be determined by observing a calibrator i.e. either an unresolved source, or a source of known diameter.

For our observations, the derivation of T_i comes from the interferometric data obtained on Arcturus. The model used to compute its theoretical visibility, the reduction method and effective wavelength determination are detailed in Sect. 4.2.

The three measurements of the transfer function on April 2 are steady within a 4% wide band, and all are above 50%. The first value, corresponding to the following night is consistent with this number of 50% (Fig. 6).

Considering that the individual components of the interferometer were not optimized for operation in the L band, and that no active polarization control was applied by macrobending of the fibers, this value of the interferometric efficiency is very encouraging. For comparison the typical value of T_i obtained in the K band with FLUOR is 70%.

4. Visibility measurements

Since our observations are limited by detector noise, we can still apply the reduction method developed for the FLUOR exper-

iment (Coudé du Foresto et al. 1997) to the L band data. Due to the effect of uncorrected atmospheric piston, object phase and spectral information are lost. The unbiased observable calculated by this method is the squared modulus of the coherence factor, derived from the energy measured in the power spectrum of the interferograms, in the frequency range of the fringes. The only difference with respect to the K band comes from the “shape factor” of the observed source in the L band (Coudé du Foresto et al. 1997). The shape factor F is given by the square of the normalized source spectrum $B(\sigma)$, integrated over the optical bandpass of the system, and is closely related to the effective wavelength of observation $\lambda_{eff}=1/\sigma_{eff}$, given by:

$$\sigma_{eff} = \frac{\int B^2(\sigma) \cdot \sigma d\sigma}{\int B^2(\sigma) d\sigma} \quad (5)$$

In practice F is mostly sensitive to the optical bandwidth, and to possible strong absorption features in the stellar atmosphere. It is otherwise roughly independent of the stellar effective temperature, and cancels out in the reduction process for objects and references of close temperatures or spectral types.

Using the transmission curve of our L band filter ($\lambda_{mean} = 3.849 \mu\text{m}$, $\Delta\lambda = 0.580 \mu\text{m}$), and a low resolution spectrum (Strecker et al. 1979) of Arcturus, we find $F=2.4 \cdot 10^{-3} \text{ cm}$, which is the value used for the absolute determination of T_i in Sect. 3.2.3., and an effective wavelength of $3.75 \mu\text{m}$. We present here the results and statistical error bars provided by this reduction method, when applied to the interferometric data obtained on Arcturus and α Her.

4.1. Using Arcturus as a calibrator

The value of the instrumental transfer function T_i is derived from the data obtained on Arcturus, used as a calibrator. In the K band, FLUOR/IOTA observations (Perrin et al. 1998) show that the uniform disk and limb darkened diameter of Arcturus already match within 3%. In the L band the limb darkening effect is expected to be still smaller, because the blackbody emission of the 4300 K star is less affected by a given thermal gradient in the stellar photosphere. Furthermore, Arcturus is very partially resolved at the spatial frequency of operation, so that taking limb darkening effects into account, the theoretical visibility departs very little from the one computed using uniform disk approximation.

To compute the expected theoretical visibility at the spatial frequency of observation, we can then neglect the limb darkening effect in a first approximation, and we use the uniform disk diameter of $20.20 \pm 0.08 \text{ mas}$ measured in the K band by the FLUOR instrument. Measured fringe contrasts on Arcturus are given in Table 3. First three batches correspond to the night of April 2, the fourth one was observed on the following night.

4.2. Deriving an angular diameter of α Her in the L band

α Her was observed 3 times in one and a half hour during the night of April 2 1998. These 3 batches have been analyzed in-

Table 2. Theoretical visibilities (V_{th}) and measured fringe contrasts μ_m on Arcturus. S (in cycles/arcsec) is the spatial frequency at the effective wavelength of observation. The adopted uniform disk diameter of Arcturus is $20.20 \pm 0.08 \text{ mas}$. First 3 batches are for the night of April 2 1998, the fourth one corresponds to April 3. Error bars correspond to the 1σ level.

Batch	S	V_{th} in%	μ_m in%	T_i in%
1	26.76	68.04 ± 0.22	35.2 ± 0.6	51.8 ± 0.8
2	26.78	67.98 ± 0.22	37.2 ± 0.6	54.8 ± 0.8
3	26.87	67.79 ± 0.22	35.0 ± 0.6	51.6 ± 0.8
4	26.76	68.04 ± 0.22	34.1 ± 0.6	50.1 ± 0.8

Table 3. Observed fringe contrasts $\mu_{\alpha Her}$, and corresponding visibility measurements $V_{\alpha Her}$ on α Her as a function of the spatial frequency S . For the 3 batches, the interferometric transfer function used is 0.516 ± 0.008 , from most recent observations of Arcturus.

Batch	S (arcsec^{-1})	$\mu_{\alpha Her}$ in%	$V_{\alpha Her}$ in%
1	26.31	18.88	36.59
2	26.16	14.74	28.56
3	26.19	17.04	33.02

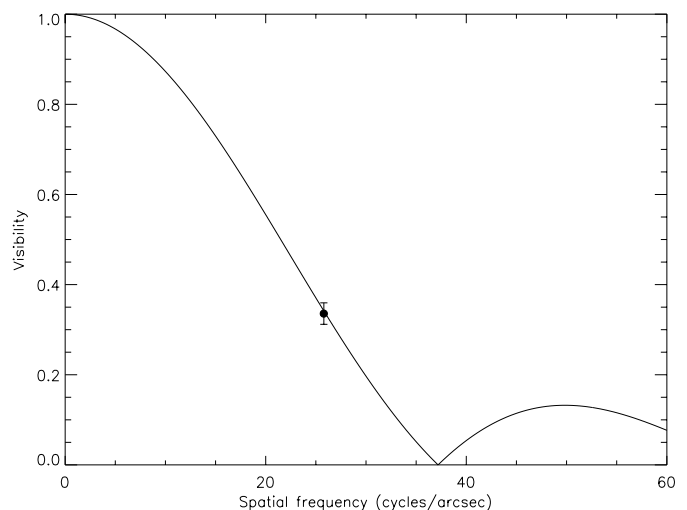


Fig. 7. Uniform disk fit for α Her in the L band. Visibility point and error bar synthesize three independent measurements at the same spatial frequency.

dependently using the sky estimation described above, and the closest most recent available value of the transfer function deduced from the observations of Arcturus ($T_i=0.516 \pm 0.011$).

Individual visibility measurements are given in Table 3. The relative dispersion of visibility measurements is about 10% rms. Since the estimation of the thermal background causes an rms error of 1% at the worst (Sect. 3.1.2), we conclude that most of the observed variations probably arise from the lack of injected flux monitor and not from unsampled background fluctuations.

These three independent measurements – assumed to be of equal quality – are used to provide a single visibility data at the mean spatial frequency of observation (minimizing a χ^2

functional). Corresponding error bar is determined so that $\chi^2 = \chi_{min}^2 + 1$.

Fitting this data point with a uniform disk model, we derive a uniform disk diameter for α Her of 32.8 ± 0.7 mas in the L band (Fig. 7).

Uniform disk diameters found in the K band by the FLUOR experiment and by the infrared Michelson array IRMA (Benson et al. 1991) are respectively: 30.90 ± 0.02 mas and 32.2 ± 0.8 mas. Favoring the more accurate results found with FLUOR, our L band measurements would then indicate a 6% increase in the photosphere diameter with respect to K observations.

5. Conclusions

The possibility to spatially filter the wavefronts in the L band and combine them coherently with low dispersion and good interferometric efficiency has been demonstrated successfully for the first time on two stars brighter than $m_L = -3$.

This first experiment in the thermal infrared looks then encouraging, and a few modifications are under way for future interferometric observations on IOTA in the L and M bands with the TISIS experiment. Using an X coupler dedicated to these wavelengths, with two optimized InSb infrared detectors should help gaining both in accuracy and sensitivity, up to the point where the thermal background will this time dominate. A dedicated chopping and nodding capability will then become mandatory.

More generally, stellar interferometric observations at these intermediate infrared wavelengths look very promising for stellar physics. For instance $5\mu\text{m}$ long baseline interferometric measurements would have sufficient resolution to directly detect the dust shell warm inner regions located typically 50 to 70 mas away from some late type stars, according to heterodyne observations at longer wavelengths. They should very well constrain envelopes inner radii, mass loss rates and mechanisms. In that sense they are very complementary to observations in K, mostly sensitive to the photosphere, and to the 11 microns observations of cooler regions in extended shells.

Acknowledgements. The authors would like to salute the memory of their friend and colleague Jean-Marie Mariotti, who died tragically in July 1998, a few months after the observations reported here were carried out.

References

- Angel J.R.P., Woolf N.J., 1997, ApJ 475, 373
 Benson J.A., Dyck H.M., Ridgway S.T., et al., 1991, AJ 102, 2091
 Carleton N.P., Traub W.A., Lacasse M.G., et al., 1994, Proc. SPIE 2200, 152
 Colavita M., Boden A.F., Crawford S.L., 1998, Proc. SPIE 3350, 776
 Coudé du Foresto V., Ridgway S., Mariotti J.M., 1997, A&A
 Coudé du Foresto V., Perrin G., Ruilier C., et al., 1998, Proc. SPIE, 3350, 854
 Danchi W.C., Bester M., Degiacomi C.G., Greenhill L.J., Townes C.H., 1994, AJ 107, 1469
 Gay J., Mékarnia D., 1988, NOAO-ESO Conference on High Resolution by Interferometric Imaging II, 811–816
 Léger A., Mariotti J.M., Mennesson B., et al., 1996, Icarus 123, 249
 Leinert C., Graser U., 1998, Proc. SPIE 3350, 389
 McCarthy D.W., Low F.J. 1975, ApJ 202, L37
 McCarthy D.W., Low F.J., Howell R., 1977, ApJ 214, L85
 Mékarnia D., Gay J., 1990, A&A 238, 469
 Mennesson B., Rviliier C., Olliver M., 1998, Journal of the Optical Society of America (in preparation)
 Millan-Gabet R., 1998, Proc. SPIE 3350, 432
 Monerie M., Alard F., Mazé G., 1985, Electronic Letters Vol. 21, No. 25/26, 1179–1181
 Neumann E.G., 1988, Single Mode Fibers. Springer-Verlag
 Natta A., 1997, In: Paresce F. (ed.) Science with the VLTI. Proceedings ESO Workshop, p. 237
 Ollivier M., Mariotti J.M., 1997, Applied Optics 36, 5340
 Perrin G., 1996, Ph.D. Dissertation
 Perrin G., Coudé du Foresto V., Ridgway S.T., et al., 1998, A&A 331, 619
 Ruilier C., 1998, Proc. SPIE 3350, 319
 Shaklan S., Roddier F., 1988, Applied Optics 27, 2234
 Strecker D.W., Erickson E.F., Witteborn F.C., 1979, ApJS 41, 501
 Traub W.A., 1998, SPIE 3350, 848
 Voit G.M., 1997, ApJ 487, L109